Geophysical Research Letters

RESEARCH LETTER
10.1029/2018GL081413

Universal Relationship Between Viscous and Inertial Permeability of Geologic Porous Media

Jia-Qing Zhou[1,2], Yi-Feng Chen[1], Lichun Wang[3], and M. Bayani Cardenas[4]

[1]State Key Laboratory of Water Resources and Hydropower Engineering Science, Wuhan University, Wuhan, China, [2]Now at Faculty of Engineering, China University of Geosciences, Wuhan, China, [3]Institute of Surface-Earth System Science, Tianjin University, Tianjin, China, [4]Geological Sciences, University of Texas at Austin, Austin, Texas, USA

Key Points:
- We analyzed and synthesized viscous and inertial permeability data for different types of geologic porous media
- A universal visco-inertial permeability model is established using the compiled data
- The parameter in the universal model is attributed to local surface roughness and void distribution pattern

Supporting Information:
- Supporting Information S1
- Table S1
- Data Set S1
- Data Set S2

Correspondence to:
Y.-F. Chen,
csyfchen@whu.edu.cn

Citation:
Zhou, J.-Q., Chen, Y.-F., Wang, L., & Cardenas, M. B. (2019). Universal relationship between viscous and inertial permeability of geologic porous media. *Geophysical Research Letters*, *46*, 1441–1448. https://doi.org/10.1029/2018GL081413

Received 5 MAY 2018
Accepted 18 JAN 2019
Accepted article online 28 JAN 2019
Published online 10 FEB 2019

Abstract Fluid flow through geologic porous media is represented by Darcy's law and its inertial and nonlinear extension, the Forchheimer equation. These relationships equate the product of the driving potential gradient and phenomenological coefficients representing momentum resistance and dissipation to flux. From decades of research, the coefficient of viscous permeability (k_v) in Darcy's law is largely predictable, but this is not the case for the coefficient of inertial permeability (k_i) in the Forchheimer equation. Synthesizing results from thousands of laboratory and field flow tests and pore-scale flow model results, we show that k_i can be predicted from k_v via the equation $k_i = 10^{10}k_v^{3/2}$ across 12 and 20 orders of magnitude in k_v and k_i, respectively. Since it is related with k_i, k_v is thus sufficient for predicting flow across viscous to inertial regimes for most geologic porous media.

Plain Language Summary Fluid flow through geologic porous media is dictated by permeability which is the resistance imparted by the medium. Flows in porous media are described by either Darcy's law or its extension for high flow rates, the Forchheimer equation. In both models, permeability represents the dissipation of mechanical energy by inertial losses and by fluid viscosity. Thus, permeability depends on both fluid properties and the configuration of pores. Decades of research has made the permeability in Darcy's law predictable from medium properties such as porosity and grain size, but the additional permeability in the Forchheimer equation has remained almost impossible to predict. This has hindered the application of the Forchheimer equation for many settings where it is potentially more appropriate. Through a broad synthesis of published data and through computational simulations, we were able to relate the permeability in Darcy's law to the permeability in the Forchheimer equation for the diversity of geologic porous media representing varied pore geometries and configurations. Thus, both kinds of permeability are now predictable and linked. This knowledge will help in many geophysical and engineering applications where it is necessary to consider flows at high rates.

1. Introduction

The ability to transmit fluids through porous and fractured media, permeability, is the most important parameter for understanding and predicting fluid flow and solute transport. Permeability thus dictates the role of subsurface fluids in many geologic phenomena such as earthquakes (Elkhoury et al., 2006), volcanic eruptions (Okumura et al., 2009), ice sheet drainage (Das et al., 2008), planetary compositional differentiation (Ghanbarzadeh et al., 2017), and weathering of the land surface (Rempe & Dietrich, 2014). Knowledge of permeability is crucial for the sustainable extraction of groundwater (Gleeson et al., 2014) and energy resources (Patzek et al., 2013), for assessing contaminant transport in and the vulnerability of aquifers (Burgess et al., 2010), and the security of potential reservoirs for nuclear waste (Ghanbarzadeh et al., 2015) and greenhouse gas disposal (Bickle, 2009). Numerous models and methods for studying permeability have therefore been developed, including some attempts for finding common attributes among geologic porous media (Bonnet et al., 2001; Liu, 2011; Pyrak-Nolte & Nolte, 2016; Wang & Cardenas, 2017; Wei et al., 2015). However, due to complicated and diverse pore and fracture geometries and highly varied hydrodynamic, mechanical, and environmental conditions, there is no universally predictive model applicable across all geologic porous media. This has remained an open fundamental problem for decades.

Darcy's law states that flow rate is linearly proportional to fluid pressure gradient; this relationship is obtained by neglecting the inertial terms in the Navier–Stokes equations, thus requiring that viscous forces dominate in energy dissipation. At higher flow rates, non-Darcian flows take place which are then described by the Forchheimer equation (Bear, 1972; Chaudhary et al., 2011; Forchheimer, 1901; Javadi et al., 2014; Liu, Li, & Jiang, 2016; Qian et al., 2007; Rust & Cashman, 2004; Zeng & Grigg, 2006; Zimmerman et al., 2004). For an incompressible fluid, the Forchheimer equation reads as

$$\frac{dp}{dl} = \frac{\mu}{k_{\mathrm{v}}} v + \frac{\rho}{k_{\mathrm{i}}} v^2 \tag{1}$$

where k_{v} and k_{i} are the viscous and the inertial permeabilities, respectively; dp/dl is the fluid pressure gradient; μ is the fluid viscosity; ρ is the fluid density; and v is the specific flux (volumetric flux per area). The Forchheimer equation reduces to Darcy's law when the inertial term, the second term in the right-hand side, becomes negligible.

Non-Darcian flow characteristics have been ascribed to the formation and growth of eddies or recirculation zones caused by significant inertial forces (Cardenas et al., 2009;Chaudhary et al., 2011; Lee et al., 2014). Eddies are persistently and distinctly separate to the bulk flow in geologic porous media, and the apparent permeability calculated from Darcy's law continuously decreases under this hydrodynamic condition (Chaudhary et al., 2013; Sivanesapillai et al., 2014; Zhou et al., 2015). Moreover, pore geometry can be varied due to external stress (Pyrak-Nolte & Nolte, 2016) and internal fluid-pressure (Watanabe et al., 2017), and processes such as chemical erosion (Deng et al., 2015), phase change (Wang & Cardenas, 2017), and degassing (Takeuchi et al., 2009), leading to various geometries and subsequently significant variation in permeability. In many situations, the inertial versus viscous force competition and geometric variation are intertwined. Investigations of hydrodynamic factors, that is, inertial effects, typically assume static pore geometry (Chaudhary et al., 2011; Lee et al., 2014). On the other hand, investigations of the effects of geometric variation, for example, due to deformation and phase change, are typically constrained to noninertial, viscous flow regimes (Pyrak-Nolte & Nolte, 2016; Wang & Cardenas, 2017). The interaction between pore geometry variation and the competition between viscous and inertial forces are the cruxes of porous and fractured media flow prediction. This study's goal is to determine a universal relationship which can describe flow or hydraulic properties across viscous and inertial regimes for all geologic porous media representing different pore geometry.

2. Methodology

Since they both represent dissipation of momentum and depend on the geometric properties of the medium, we postulate that k_{i} and k_{v} are functionally related. Since the units of k_{i} and k_{v} are m and m^2, respectively, we initially expect that $k_{\mathrm{i}} \sim {k_{\mathrm{v}}}^{1/2}$ based on dimensionality. This can be generalized into the heuristic model:

$$k_{\mathrm{i}} = \omega {k_{\mathrm{v}}}^{\alpha/2} \tag{2}$$

with the scaling coefficient ω having units of $\mathrm{m}^{(1-\alpha)}$. Note that the power law relationship with different coefficient ω and exponent α for permeabilities (k_{v}, k_{i}) has been reported in many practical problems based on a small group of samples, including for porous media (Ghane et al., 2014), single fractures (Zhou et al., 2015), fracture networks (Cherubini et al., 2012), and fractured porous media (Chen, Hu, et al., 2015). Here we seek a universal power law relationship for the entirety of geologic porous media.

The scale coefficient ω and the factor in the exponent α need to be determined empirically or mechanistically. This study applies both empirical and mechanistic approaches to determine the scale factor and the exponent. For any empirical relationship to be considered "universal," a wide variety and large number of geologic porous media must be collected and analyzed comprehensively (Pyrak-Nolte & Nolte, 2016). An exhaustive compilation and analysis of data available from literature was thus conducted. This represents data from flow tests of a vast array of geologic porous media including some engineered or synthetic "geologic" porous media. Sources include scores of studies representing thousands of laboratory, field, and digital flow tests, with study scales spanning from individual pores, to pore networks, to core samples, and to field-scale situations (see legends in Figure 1 and see Table S1 in the supporting information for the data sources). Since all the flow data were obtained from physical experiments (laboratory and field) or by numerical simulations that directly solve the Navier–Stokes equations (more on this below), they reflect true flow conditions in geologic porous media. Some sources already reported k_{v} and k_{i} values, whereas others provided raw flow

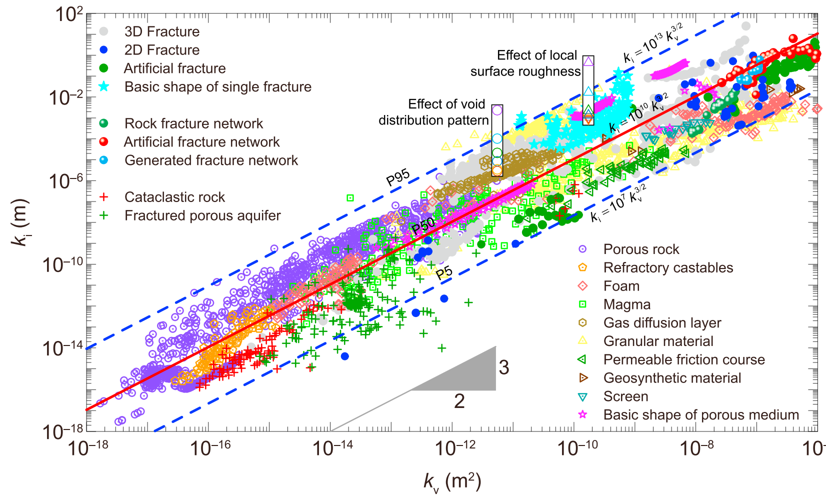

Figure 1. Compilation of permeability for diverse geologic porous media. The geologic porous media can be grouped into four categories according to their geometric features: single fractures (solid dots), porous media (hollow dots), fracture networks (spherical dots), and fractured porous media (vertical crosses). Each category contains several subcategories, denoted using different colors or shapes. The data came from detailed research and analysis of the flow information reported in the literature, involving more than 100 papers and 4,000 geologic or analogous-geologic porous medium samples. The detailed statistical information of the data including sources and values are provided in Tables S1–S3 in the supporting information, respectively. The compilation shows that collectively the geologic porous media follow the power law with exponent of 3/2 (red line). The compilation exhibits large scatter for each geologic porous medium (dashed blue lines represent 95% prediction bounds, where P is the percentile distribution), which is ascribed to local surface attributes and void distribution patterns. The data in the rectangular boxes are used to discuss the roles of local surface roughness and void distribution pattern in determination of permeability (k_v, k_i).

test data, that is, pressure-flow rate curves. In the cases of the latter, the Forchheimer equation was fitted to obtain permeabilities (k_v, k_i). Details on the methodologies for different cases are provided in Text S1 in the supporting information (American Society for Testing and Materials International, 2001; Barker, 1988; Chen, Liu, et al., 2015; Gurau et al., 2007; Liao et al., 2016; Liu, Chen, et al., 2016; Pant et al., 2011; Quinn et al., 2011; Ranjith & Darlington, 2007).

In equation (2), k_i, representing nonlinear momentum dissipation, is the dependent variable. We chose this form since k_v, representing viscous resistance, has been studied extensively and is predictable from basic geometric properties such as pore (or grain size) diameter, fracture aperture, and bulk porosity. To further analyze equation (2), we focused on the previously published experiments or simulations that have individually assessed pore shape variation's effects on flow via physical processes (see illustrations in Figure 2), where the permeabilities change in magnitude with the geologic porous media having geometric similarities (varying from the same initial geometry).

We also conducted computational fluid dynamics (CFD) modeling of flow through idealized axis-symmetric pores (see illustrations in Figure 3) whose geometry was then systematically varied by changing the pore radii. We then expounded and expanded on the results of initial models via additional simulations and through analysis of previously published experiments wherein the pore geometry of the media varied from some same initial geometry. Finally, all the CFD modeling results were synthesized along with those from scores of previous reports representing viscous to inertial flow regimes and most geologic and some engineered porous media representing 2-D/3-D pores and porous media, 2-D/3-D fractures, natural and synthetic pore and fracture networks, foam, magma, and screens.

In the CFD modeling, we first investigated an idealized pore geometry with sinusoidal walls in an axis-symmetric framework (Figure 3a), following previous investigations where basic pore configurations were adopted to reveal the underlying physical mechanism for complex flow and transport phenomena (Bolster et al., 2014; Veyskarami et al., 2016). The pore geometry can be fully characterized by two dimensionless numbers, the aspect ratio (L/R_t) and fluctuation (R_b/R_t), where L is the longitudinal length of the pore and R_t and R_b are the radii at the pore throat and pore body, respectively. To consider a wide range of

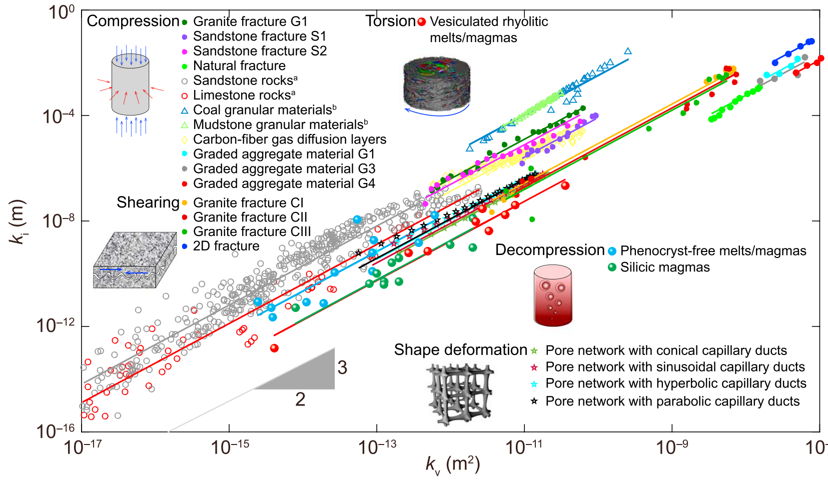

Figure 2. Permeability variation for different sets of processes driving pore geometry variation. Each data set can be treated as a continuous evolution of permeability during different geophysical processes, including compression, shearing, torsion, decompression, and designed shape deformation. The data sets all follow the power law with exponent of 3/2 (solid lines), similar to the trend revealed by the synthesis presented in Figure 1. Details on the data set including geologic porous media, geophysical processes, and fitted parameters are provided in Table S4 in the supporting information. Illustrations of torsion and shape deformation in the figure are taken from Okumura et al. (2009) and Veyskarami et al. (2016), respectively. [a]Original data could not be distinguished and thus contain more than one medium. [b]More than one medium due to overlap of the data points, a better illustration for each medium is provided in Figure S2 in the supporting information.

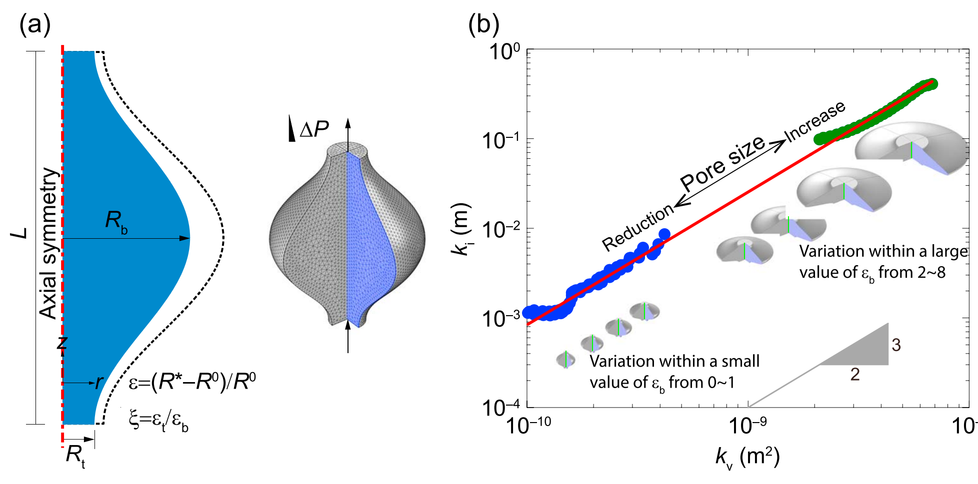

Figure 3. Pore-scale modeling of visco-inertial permeability dependence on geometry variation. (a) Design of idealized pores and definition of parameters which describe geometry variation. The idealized pore has an axisymmetric sinusoidal geometry characterized by pore body (divergence zone) and throat (convergence zone) with radii, R_b and R_t, respectively. By changing parameter ε of the body and throat and parameter ξ between them, a series of altered geometries can be generated. R^* and R^0 are the throats after and before deformation, respectively. ε_b and ε_t represent the parameter ε at the pore body and throat, respectively. The inset shows a full 3-D pore geometry. (b) Permeability (k_v, k_i) estimated from a series of pore size reductions and increases for the idealized pore, based on the computational fluid dynamics (CFD) simulation. The left blue circles in (b) correspond to geometry variation within a small value of ε_b from 0 to 1, while the right green circles correspond to geometry variation within a large value of ε_b from 2 to 8. Typical pore shapes are illustrated in left bottom and right top of (b) at the same scale, for these two suites of geometry variation. CFD simulations were conducted at different ranges of Reynolds number for these two cases to ensure inertial but not turbulent flow (see Text S3 in the supporting information). The permeability evolution of k_v-k_i is characterized by a power law with an exponent of 3/2.

different pore sizes and geometries, we introduce two more geometric parameters, that is, $\varepsilon = (R^* - R^0)/R^0$ and $\xi = \varepsilon_t/\varepsilon_b$. R^* and R^0 are the radii after and before the geometry variation, respectively, and ε_t and ε_b correspond to the parameter ε of R_t and R_b, respectively. By setting L/R_t and R_b/R_t, an initial pore geometry can be designed, and following this by prescribing ε_b and ξ, a suite of different geometry can be generated (see Text S2 in the supporting information for details of the pore generation). To obtain a wide range of k_v-k_i pairs, we generated two suites of pore geometries where both geometric parameters were originated from the same initial pore ($R_t = 1 \times 10^{-5}$ m, $L/R_t = 10$, $R_b/R_t = 5$); one suite was varied within a small value of ε_b from 0 to 1 (typical shapes illustrated in left bottom of Figure 3b) while another varied within a large value of ε_b from 2 to 8 (typical shapes illustrated in right top of Figure 3b).

CFD simulations of steady flow with increasing dp/dl were conducted for the systematically varied pore geometry to obtain dp/dl-v curves. Reynolds number $Re = 100$ and $Re = 4$ was set as the upper limit of Re for these CFD simulations of geometry variation within small and large ε_b, respectively, to avoid conditions where the inertial flow is not well developed or where it might be turbulent (see Text S3 in the supporting information for additional discussion on the hydrodynamic conditions with related references [Zou et al., 2015; Zhou et al., 2018, 2019]). Re is defined as $\rho v R_t/\mu$. Fitting each curve with equation (1) gives a k_v-k_i pair. Further details of the pore-scale CFD simulations are provided in Text S2 in the supporting information (Ferziger & Peric, 2002; Roache, 1998; Sahimi, 2011).

3. Results and Discussion

Analysis of the extensive data set on flow tests available in the literature shows that the Forchheimer equation fits all the data reasonably well. The compiled results of k_v-k_i pairs are presented in Figure 1, where a total of more than 4,000 k_v-k_i pairs from more than 100 previous studies representing a diverse range of geologic porous media were synthesized (the complete data sets in the form of k_v-k_i pairs are provided in Table S2 in the supporting information, while original data sets in the form of pressure-flow rate curves are provided in Table S3 in the supporting information). These results include those from synthetic materials (e.g., foams and screens) and additional results discussed later (presented in Figures 2 and 3). The media were grouped into four categories including two more basic ones, that is, porous media and single fractures, and two combinations of them, that is, fracture networks and fractured porous media.

There is a wide distribution of k_v-k_i in geologic (and synthetic) porous media, with k_v varying over 12 orders of magnitude (10^{-18}–10^{-6} m^2) and k_i over 20 orders of magnitude (10^{-18}–10^2 m). Even for a specific category, large scatter was observed. However, the synthesis shows that the heuristic power law model of equation (2) is true for and covers all geologic porous media. Fitting equation (2) to all the data leads to $\alpha \approx 3$ (precisely 2.96) and $\omega \approx 10^{10}$ m^{-2} with lower and upper bounds of 10^7 m^{-2} and 10^{13} m^{-2}, respectively (Figure 1). A universal model for hydraulic properties is hence established. Once a medium has a known k_v, one can estimate k_i with reasonable statistical uncertainty. The calculation of flow through any geologic porous medium from viscous to inertial regimes is now possible given estimates of k_i.

To further establish whether equation (2) suitably describes real geologic porous media representing different processes inducing pore geometry variation, we focused on the results from groups of previous laboratory experiments where geologic samples were deformed through compression (Dan et al., 2016; Gostick et al., 2006; Jones, 1987; Ma et al., 2015; Ma et al., 2016; Schrauf & Evans, 1986; Zhou et al., 2015), torsion (Okumura et al., 2009), shearing (Javadi et al., 2014; Wang, 2017), or decompression (Lindoo et al., 2016; Takeuchi et al., 2009), and from modeling experiments where pore networks with ducts of different shapes were systematically varied (Veyskarami et al., 2016), like we did with our CFD simulations discussed below. The complete details on the data set including the type of geologic porous media, the geometry-varying processes represented, and the fitted parameters are provided in Table S4 in the supporting information.

The subgrouped compilation (Figure 2) shows that each experimental set follows the power law scaling (equation (2)) with an exponent of 3/2, with $R^2 = 0.65$–0.99 (see Table S4 in the supporting information). The geologic porous media represented by the subgrouped studies were subject to significant geometric variation as they underwent the geometry-varying process. Given this, it is not surprising that these geologic porous media exhibited significant variations in k_v-k_i. The relationship between k_v and k_i for these subgrouped geologic porous media with geometric similarities followed the 3/2 power law scaling nonetheless. Thus, the 3/2 exponent appears universal, and may hold for a diverse range of geologic porous media samples. It is also further shown that ω covers a broad range and that it is potentially medium- or geometry-specific.

To further test whether the power law scaling is physically plausible for conceptual models of geologic porous media, we turn to CFD model experiments of systematically varied idealized 3-D axisymmetric pores. Two suites of CFD simulation experiments were conducted—representing pore size reduction and increase (Figure 3b). Note that the CFD simulations were implemented in an axis-symmetric framework, and thus, the flow process was quasi-3D where the prevalence and magnitude of eddies (responsible for the occurrence of non-Darcian flow behavior) may differ from ones in real, complex 3-D flows (Crevacore et al., 2016; Lee et al., 2015). The resulting k_v-k_i pairs (left blue circles correspond to geometry variation within a small ε_b, while right green circles correspond to large ε_b) from the suites of CFD simulations yielded the same power law relationship (equation (2)) with an exponent of 3/2. Each k_v-k_i pair, which is also included in Figure 1, represents a series of flow simulations that determine a pressure gradient-flow rate curve analyzed with equation (1). These mechanistic simulation results support the heuristic model (equation (2)). The positive association between permeabilities (k_v, k_i) is also physically meaningful, as larger k_v is usually accompanied by smaller flow resistance which results in smaller inertial energy dissipation and thus larger k_i.

The power law scaling with a final exponent of 3/2 reasonably describes a universal flow law for geometrically variable geologic porous media. However, ω could vary over several orders of magnitude for different geologic porous media (Figures 1 and 2). A quantitative estimation and characterization of ω is not trivial, given that ω itself is a highly generalized coefficient where both medium geometry and flow regime evolve. This brings up the question of: for a specific k_v, why does k_i vary several orders of magnitude? To address this question, the physical meaning of these two permeabilities needs to be revisited.

Both k_v and k_i are continuum properties of a medium founded on the same microscale physics, but on different aspects of the microscale processes. k_v and k_i describe the energy losses caused by viscous and inertial dissipation mechanisms, respectively, which together determine the apparent permeability ($k_a = \mu v/\nabla p$) of the medium. Apart from connectivity, k_v is more related to bulk geometric properties like porosity and aperture (i.e., void volume), while k_i is perhaps more related to the arrangement of pores and tortuosity (i.e., void pattern). Based on this intuition and via some additional CFD simulations of specifically designed geologic porous media to address this issue, we found that the answer to the question above comes down to different local surface roughnesses and void distribution patterns. The role of local surface roughness was scrutinized with a set of diverging–converging pores with the same large-scale waviness (aspect ratio = 5 and fluctuation = 10) and k_v but different local surface roughness (see Figure S3 in the supporting information). The role of void distribution pattern was tested with a set of porous media with the same porosity (53.8%) and k_v but different void distribution patterns (see Figure S5 in the supporting information). Note that the same k_v value was guaranteed by using a strategy of repeatedly adjusting the overall size of these geometries (with the obtained scaling adjustment factors shown in Figures S3 and S5 in the supporting information), given that k_v is mainly dependent on the void volume or geometry size. The CFD simulations of these cases show that a medium could have k_i varying 3 orders of magnitude simply due to different local surface roughnesses or void distribution patterns (depicted in Figure 1; also see Figures S4 and S6 in the supporting information for details). Given the potential diversity in local surface roughness and the potential complexity in void distribution pattern for natural or engineered geologic porous media, large difference in ω is thus not surprising. Text S4 in the supporting information provides the details of the additional CFD simulations and discussions with related references (Costa, 2006; International Society of Rock Mechanics, 1978).

The role of the local surface roughness and void distribution pattern in determining ω has a physical basis. The rock type, particle size, and presence of surface skin as well as its degree of weathering combine to shape local surface roughness of the pore or fracture walls. This local surface roughness may not change significantly for a group of media with geometric similarities and also obviously for a specific medium (shown in Figures 2 and 3). Similarly, while porosity can change much due to geometrical variation for a group of media with geometric similarities or for a specific medium, the void distribution pattern may remain more similar. Therefore, the local surface roughness and void distribution pattern may contribute to the parameter ω, which could be partially responsible for the huge scatter in Figure 1. We thus recommend further efforts to more broadly understand the meaning of ω and further collapse the permeability data into a narrower distribution by introducing some highly generalized and hopefully predictable parameters.

4. Conclusions

We present a power law scaling relationship between viscous and inertial permeabilities in geologic porous media, based on results from a vast number of laboratory and field observations and pore-scale flow simulations. This visco-inertial permeability model universally describes the consistency of the scaling across a diverse range of geologic media. The findings establish a framework for permeability estimation of diverse geologic porous media, and can serve as a foundation for non-Darcian flow parameterization and modeling when inertial effects become significant.

Acknowledgments
The authors gratefully thank Editor-in-Chief Noah Diffenbaugh and the two anonymous reviewers for their valuable and constructive comments in improving this study. This work was supported by the National Natural Science Foundation of China (grant 51579188) and as part of the Center for Frontiers of Subsurface Energy Security (CFSES) at the University of Texas at Austin, an Energy Frontier Research Center funded by the U.S. Department of Energy, Office of Science, and Office of Basic Energy Sciences under award DE-SC0001114. The first author acknowledges support from the China Scholarship Council. All original data used for plotting and analyzing can be found in the supporting information.

References

American Society for Testing and Materials International (2001). *Standard Test Method for Permeability of Rocks by Flowing Air*, *Stand. D4525–04*. West Conshohocken, PA: ASTM International.

Barker, J. (1988). A generalized radial flow model for hydraulic tests in fractured rock. *Water Resources Research*, *24*(10), 1796–1804. https://doi.org/10.1029/WR024i010p01796

Bear, J. (1972). *Dynamics of Fluids in Porous Media*. New York: American Elsevier.

Bickle, M. J. (2009). Geological carbon storage. *Nature Geoscience*, *2*(12), 815–818. https://doi.org/10.1038/ngeo687

Bolster, D., Méheust, Y., Le Borgne, T., Bouquain, J., & Davy, P. (2014). Modeling preasymptotic transport in flows with significant inertial and trapping effects—The importance of velocity correlations and a spatial Markov model. *Advances in Water Resources*, *70*, 89–103. https://doi.org/10.1016/j.advwatres.2014.04.014

Bonnet, E., Bour, O., Odling, N. E., Davy, P., Main, I., Cowie, P., & Berkowitz, B. (2001). Scaling of fracture systems in geological media. *Reviews of Geophysics*, *39*(3), 347–383. https://doi.org/10.1029/1999RG000074

Burgess, W. G., Hoque, M. A., Michael, H. A., Voss, C. I., Breit, G. N., & Ahmed, K. M. (2010). Vulnerability of deep groundwater in the Bengal aquifer system to contamination by arsenic. *Nature Geoscience*, *3*(2), 83–87. https://doi.org/10.1038/ngeo750

Cardenas, M. B., Slottke, D. T., Ketcham, R. A., & Sharp, J. M. (2009). Effects of inertia and directionality on flow and transport in a rough asymmetric fracture. *Journal of Geophysical Research*, *114*, B06204. https://doi.org/10.1029/2009JB006336

Chaudhary, K., Cardenas, M. B., Deng, W., & Bennett, P. C. (2011). The role of eddies inside pores in the transition from Darcy to Forchheimer flows. *Geophysical Research Letters*, *38*, L24405. https://doi.org/10.1029/2011GL050214

Chaudhary, K., Cardenas, M. B., Deng, W., & Bennett, P. C. (2013). Pore geometry effects on intrapore viscous to inertial flows and on effective hydraulic parameters. *Water Resources Research*, *49*, 1149–1162. https://doi.org/10.1002/wrcr.20099

Chen, Y., Hu, S., Hu, R., & Zhou, C. (2015). Estimating hydraulic conductivity of fractured rocks from high-pressure packer tests with an Izbash's law-based empirical model. *Water Resources Research*, *51*, 2096–2118. https://doi.org/10.1002/2014WR016458

Chen, Y. F., Liu, M. M., Hu, S. H., & Zhou, C. B. (2015). Non-Darcy's law-based analytical models for data interpretation of high-pressure packer tests in fractured rocks. *Engineering Geology*, *199*, 91–106. https://doi.org/10.1016/j.enggeo.2015.10.011

Cherubini, C., Giasi, C., & Pastore, N. (2012). Bench scale laboratory tests to analyze non-linear flow in fractured media. *Hydrology and Earth System Sciences*, *16*(8), 2511–2522. https://doi.org/10.5194/hess-16-2511-2012

Costa, A. (2006). Permeability-porosity relationship: A reexamination of the Kozeny-Carman equation based on a fractal pore-space geometry assumption. *Geophysical Research Letters*, *33*, L02318. https://doi.org/10.1029/2005GL025134

Crevacore, E., Tosco, T., Sethi, R., Boccardo, G., & Marchisio, D. L. (2016). Recirculation zones induce non-Fickian transport in three-dimensional periodic porous media. *Physical Review E*, *94*(5), 053118. https://doi.org/10.1103/PhysRevE.94.053118

Dan, H. C., He, L. H., & Xu, B. (2016). Experimental investigation on non-Darcian flow in unbound graded aggregate material of highway pavement. *Transport in Porous Media*, *112*(1), 189–206. https://doi.org/10.1007/s11242-016-0640-z

Das, S. B., Joughin, I., Behn, M. D., Howat, I. M., King, M. A., Lizarralde, D., & Bhatia, M. P. (2008). Fracture propagation to the base of the Greenland ice sheet during supraglacial lake drainage. *Science*, *320*(5877), 778–781. https://doi.org/10.1126/science.1153360

Deng, H., Fitts, J. P., Crandall, D., McIntyre, D., & Peters, C. A. (2015). Alterations of fractures in carbonate rocks by CO_2-acidified brines. *Environmental Science & Technology*, *49*(16), 10,226–10,234. https://doi.org/10.1021/acs.est.5b01980

Elkhoury, J. E., Brodsky, E. E., & Agnew, D. C. (2006). Seismic waves increase permeability. *Nature*, *441*(7097), 1135–1138. https://doi.org/10.1038/nature04798

Ferziger, J. H., & Peric, M. (2002). *Computational methods for fluid dynamics* (3rd ed.). Berlin, Heidelberg, New York: Springer.

Forchheimer, P. (1901). Wasserbewegung durch boden. *Zeitschrift des Vereins deutscher Ingenieure*, *45*, 1782–1788.

Ghanbarzadeh, S., Hesse, M. A., & Prodanović, M. (2017). Percolative core formation in planetesimals enabled by hysteresis in metal connectivity. *Proceedings of the National Academy of Sciences*, *114*(51), 13,406–13,411. https://doi.org/10.1073/pnas.1707580114

Ghanbarzadeh, S., Hesse, M. A., Prodanović, M., & Gardner, J. E. (2015). Deformation-assisted fluid percolation in rock salt. *Science*, *350*(6264), 1069–1072. https://doi.org/10.1126/science.aac8747

Ghane, E., Fausey, N. R., & Brown, L. C. (2014). Non-Darcy flow of water through woodchip media. *Journal of Hydrology*, *519*, 3400–3409. https://doi.org/10.1016/j.jhydrol.2014.09.065

Gleeson, T., Moosdorf, N., Hartmann, J., & Beek, L. P. H. V. (2014). A glimpse beneath Earth 's surface: GLobal HYdrogeology MaPS (GLHYMPS) of permeability and porosity. *Geophysical Research Letters*, *41*, 3891–3898. https://doi.org/10.1002/2014GL059856

Gostick, J. T., Fowler, M. W., Pritzker, M. D., Ioannidis, M. A., & Behra, L. M. (2006). In-plane and through-plane gas permeability of carbon fiber electrode backing layers. *Journal of Power Sources*, *162*(1), 228–238. https://doi.org/10.1016/j.jpowsour.2006.06.096

Gurau, V., Bluemle, M. J., Castro, E. S. D., Tsou, Y. M., Jr, T. A. Z., & Jr, J. A. M. (2007). Characterization of transport properties in gas diffusion layers for proton exchange membrane fuel cells: 2. Absolute permeability. *Journal of Power Sources*, *165*(2), 793–802. https://doi.org/10.1016/j.jpowsour.2006.12.068

International Society of Rock Mechanics (1978). Suggested methods for the quantitative description of discontinuities in rock masses. *International Journal of Rock Mechanics and Mining Sciences*, *15*, 319–368.

Javadi, M., Sharifzadeh, M., Shahriar, K., & Mitani, Y. (2014). Critical Reynolds number for nonlinear flow through rough-walled fractures: The role of shear processes. *Water Resources Research*, *50*, 1789–1804. https://doi.org/10.1002/2013WR014610

Jones, S. (1987). Using the inertial coefficient, β, to characterize heterogeneity in reservoir rock. Paper presented at SPE Annual Technical Conference and Exhibition, Society of Petroleum Engineers.

Lee, S. H., Lee, K. K., & Yeo, I. W. (2014). Assessment of the validity of stokes and Reynolds equations for fluid flow through a rough-walled fracture with flow imaging. *Geophysical Research Letters*, *41*, 4578–4585. https://doi.org/10.1002/2014GL060481
Lee, S. H., Yeo, I. W., Lee, K. K., & Detwiler, R. L. (2015). Tail shortening with developing eddies in a rough-walled rock fracture. *Geophysical Research Letters*, *42*, 6340–6347. https://doi.org/10.1002/2015GL065116
Liao, Y., Li, X., Zhong, W., & Tao, G. (2016). Study of pressure drop-flow rate and flow resistance characteristics of heated porous materials under local thermal non-equilibrium conditions. *International Journal of Heat and Mass Transfer*, *102*, 528–543. https://doi.org/10.1016/j.ijheatmasstransfer.2016.05.101
Lindoo, A., Larsen, J., Cashman, K., Dunn, A., & Neill, O. (2016). An experimental study of permeability development as a function of crystal-free melt viscosity. *Earth and Planetary Science Letters*, *435*, 45–54. https://doi.org/10.1016/j.epsl.2015.11.035
Liu, H. H. (2011). A note on equations for steady-state optimal landscapes. *Geophysical Research Letters*, *38*, L10402. https://doi.org/10.1029/2011GL047619
Liu, M. M., Chen, Y. F., Hong, J. M., & Zhou, C. B. (2016). A generalized non-Darcian radial flow model for constant rate test. *Water Resources Research*, *52*, 9325–9343. https://doi.org/10.1002/2016WR018963
Liu, R. C., Li, B., & Jiang, Y. J. (2016). Critical hydraulic gradient for nonlinear flow through rock fracture networks: The roles of aperture, surface roughness, and number of intersections. *Advances in Water Resources*, *88*, 53–65. https://doi.org/10.1016/j.advwaters.2015.12.002
Ma, D., Bai, H., Chen, Z., & Pu, H. (2015). Effect of particle mixture on seepage properties of crushed mudstones. *Transport in Porous Media*, *108*(2), 257–277. https://doi.org/10.1007/s11242-015-0473-1
Ma, D., Miao, X. X., Wu, Y., Bai, H. B., Wang, J. G., Rezania, M., et al. (2016). Seepage properties of crushed coal particles. *Journal of Petroleum Science and Engineering*, *146*, 297–307. https://doi.org/10.1016/j.petrol.2016.04.035
Okumura, S., Nakamura, M., Takeuchi, S., Tsuchiyama, A., Nakano, T., & Uesugi, K. (2009). Magma deformation may induce non-explosive volcanism via degassing through bubble networks. *Earth and Planetary Science Letters*, *281*(3-4), 267–274. https://doi.org/10.1016/j.epsl.2009.02.036
Pant, L. M., Mitra, S. K., & Secanell, M. (2011). Mass transport measurements in porous transport layers of a PEM fuel cell. Paper presented at ASME 2011 International Conference on Nanochannels, Microchannels, and Minichannels.
Patzek, T. W., Male, F., & Marder, M. (2013). Gas production in the Barnett shale obeys a simple scaling theory. *Proceedings of the National Academy of Sciences*, *110*(49), 19,731–19,736. https://doi.org/10.1073/pnas.1313380110
Pyrak-Nolte, L. J., & Nolte, D. D. (2016). Approaching a universal scaling relationship between fracture stiffness and fluid flow. *Nature Communications*, *7*, 10663. https://doi.org/10.1038/Ncomms10663
Qian, J., Zhan, H., Luo, S., & Zhao, W. (2007). Experimental evidence of scale-dependent hydraulic conductivity for fully developed turbulent flow in a single fracture. *Journal of Hydrology*, *339*(3-4), 206–215. https://doi.org/10.1016/j.jhydrol.2007.03.015
Quinn, P. M., Parker, B. L., & Cherry, J. A. (2011). Using constant head step tests to determine hydraulic apertures in fractured rock. *Journal of Contaminant Hydrology*, *126*(1-2), 85–99. https://doi.org/10.1016/j.jconhyd.2011.07.002
Ranjith, P. G., & Darlington, W. (2007). Nonlinear single-phase flow in real rock joints. *Water Resources Research*, *43*, W09502. https://doi.org/10.1029/2006WR005457
Rempe, D. M., & Dietrich, W. E. (2014). A bottom-up control on fresh-bedrock topography under landscapes. *Proceedings of the National Academy of Sciences*, *111*(18), 6576–6581. https://doi.org/10.1073/pnas.1404763111
Roache, P. J. (1998). *Verification and Validation in Computational Science and Engineering*. Albuquerque, NM: Hermosa.
Rust, A., & Cashman, K. V. (2004). Permeability of vesicular silicic magma: Inertial and hysteresis effects. *Earth and Planetary Science Letters*, *228*(1-2), 93–107. https://doi.org/10.1016/j.epsl.2004.09.025
Sahimi, M. (2011). *Flow and Transport in Porous Media and Fractured Rock: From Classical Methods to Modern Approaches*. Weinheim, Germany: John Wiley & Sons. https://doi.org/10.1002/9783527636693
Schrauf, T., & Evans, D. (1986). Laboratory studies of gas flow through a single natural fracture. *Water Resources Research*, *22*(7), 1038–1050. https://doi.org/10.1029/WR022i007p01038
Sivanesapillai, R., Steeb, H., & Hartmaier, A. (2014). Transition of effective hydraulic properties from low to high Reynolds number flow in porous media. *Geophysical Research Letters*, *41*, 4920–4928. https://doi.org/10.1002/2014GL060232
Takeuchi, S., Tomiya, A., & Shinohara, H. (2009). Degassing conditions for permeable silicic magmas: Implications from decompression experiments with constant rates. *Earth and Planetary Science Letters*, *283*(1-4), 101–110. https://doi.org/10.1016/j.epsl.2009.04.001
Veyskarami, M., Hassani, A. H., & Ghazanfari, M. H. (2016). Modeling of non-Darcy flow through anisotropic porous media: Role of pore space profiles. *Chemical Engineering Science*, *151*, 93–104. https://doi.org/10.1016/j.ces.2016.05.020
Wang, L., & Cardenas, M. B. (2017). Linear permeability evolution of expanding conduits due to feedback between flow and fast phase change. *Geophysical Research Letters*, *44*, 4116–4123. https://doi.org/10.1002/2017GL073161
Wang, M. (2017). Micro-macro characterization on flow and heat transfer in geomaterials, (PhD thesis,). Wuhan Univeristy.
Watanabe, N., Egawa, M., Sakaguchi, K., Ishibashi, T., & Tsuchiya, N. (2017). Hydraulic fracturing and permeability enhancement in granite from subcritical/brittle to supercritical/ductile conditions. *Geophysical Research Letters*, *44*, 5468–5475. https://doi.org/10.1002/2017GL073898
Wei, W., Cai, J., Hu, X., & Han, Q. (2015). An electrical conductivity model for fractal porous media. *Geophysical Research Letters*, *42*, 4833–4840. https://doi.org/10.1002/2015GL064460
Zeng, Z., & Grigg, R. (2006). A criterion for non-Darcy flow in porous media. *Transport in Porous Media*, *63*(1), 57–69. https://doi.org/10.1007/s11242-005-2720-3
Zhou, J. Q., Hu, S. H., Fang, S., Chen, Y. F., & Zhou, C. B. (2015). Nonlinear flow behavior at low Reynolds numbers through rough-walled fractures subjected to normal compressive loading. *International Journal of Rock Mechanics and Mining Sciences*, *80*, 202–218. https://doi.org/10.1016/j.ijrmms.2015.09.027
Zhou, J. Q., Wang, L., Chen, Y. F., & Cardenas, M. B. (2019). Mass transfer between recirculation and main flow zones: Is physically-based parameterization possible? *Water Resources Research*, *55*. https://doi.org/10.1029/2018WR023124
Zhou, J. Q., Wang, M., Wang, L. C., Chen, Y. F., & Zhou, C. B. (2018). Emergence of nonlinear laminar flow in fractures during shear. *Rock Mechanics and Rock Engineering*, *51*(11), 3635–3643. https://doi.org/10.1007/s00603-018-1545-7
Zimmerman, R. W., Al-Yaarubi, A., Pain, C. C., & Grattoni, C. A. (2004). Non-linear regimes of fluid flow in rock fractures. *International Journal of Rock Mechanics and Mining Sciences*, *41*, 163–169. https://doi.org/10.1016/j.ijrmms.2004.03.036
Zou, L., Jing, L., & Cvetkovic, V. (2015). Roughness decomposition and nonlinear fluid flow in a single rock fracture. *International Journal of Rock Mechanics and Mining Sciences*, *228*(1-2), 93–107. https://doi.org/10.1016/j.epsl.2004.09.025